ACS Sustainable Chemistry & Engineering

Research Article

Cite This: ACS Sustainable Chem. Eng. XXXX, XXX, XXX−XXX

pubs.acs.org/journal/ascecg

Effects of Cu−Ni Bimetallic Catalyst Composition and Support on Activity, Selectivity, and Stability for Furfural Conversion to 2-Methyfuran

Bhogeswararao Seemala,[†,‡] Charles M. Cai,[†,‡] Rajeev Kumar,[†,‡] Charles E. Wyman,[†,‡] and Phillip Christopher*[,‡,§,∥]

[†]Bourns College of Engineering - Center for Environmental and Research Technology (CE-CERT), University of California, Riverside, 1084 Columbia Avenue, Riverside, California 92507, United States

[‡]Department of Chemical and Environmental Engineering, Bourns College of Engineering, [§]Program in Materials Science, and [∥]UCR Center for Catalysis, University of California, Riverside, 900 University Avenue, Riverside, California 92521, United States

Supporting Information

ABSTRACT: Supported bimetallic catalysts have been demonstrated to enhance catalytic activity, product selectivity, and catalyst stability over supported monometallic catalysts for a range of catalytic reactions. However, the surface structure and composition of bimetallic particles can differ significantly from the bulk due to variations in surface energies and interactions with adsorbates, making the design of bimetallic catalysts with targeted properties and reactivities challenging. We report here the influence of catalyst support (Al_2O_3 and TiO_2) on the surface composition and structure of bimetallic Cu−Ni nanoparticles with varying Ni weight loading (0, 0.5, 1.5, 3, 5, and 10 wt %) at a constant Cu loading of 5 wt % and a correlation to catalytic reactivity and stability in furfural (FF) hydrodeoxygenation (HDO). Analysis via depth-profiling X-ray photoelectron spectroscopy suggested that over a range of Ni compositions in Cu−Ni/Al_2O_3 catalysts, Cu and Ni were distributed evenly within bimetallic particles, although Cu and Ni segregated into contiguous monometallic domains at the particle surfaces. In contrast, on Cu−Ni/TiO_2 catalysts near surface alloys formed, which were enriched in Cu at the particle surfaces and exposed only dispersed Ni species. The difference in compositional structure of the Cu−Ni particles on TiO_2 and Al_2O_3 was attributed to strong and specific interactions between Ni and TiO_2. On both supports the addition of Ni to Cu catalysts resulted in enhancements in the rate of FF HDO, although Al_2O_3 supported bimetallic catalysts promoted hydrogenation of the furan ring, forming mostly furfural alcohol and tetrahydrofurfuryl alcohol, while TiO_2 supported catalysts mostly resulted in carbonyl hydrogenolysis to form methyl furan (MF). Through optimization of support and bimetallic compositions, low-cost bimetallic catalysts were developed that demonstrated >90% MF yields in FF HDO with good stability and regenerability.

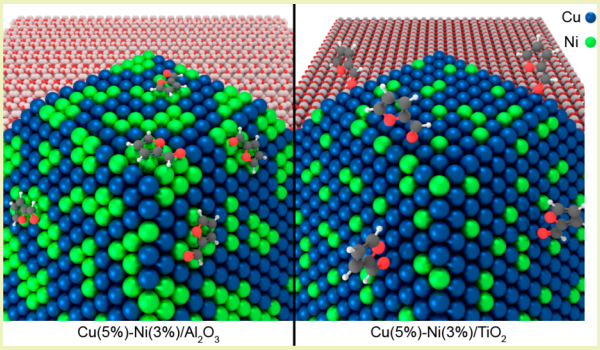

KEYWORDS: *Hydrodeoxygenation, Bimetallic catalysts, Metal−support interactions, Biofuels, Heterogeneous catalysis*

INTRODUCTION

Oxide-supported bimetallic heterogeneous catalysts consisting of late-transition and noble metals play a significant role in chemical transformations, with demonstrated enhancements in catalytic activity, product selectivity, and catalyst stability as compared to supported monometallic catalysts.[1−5] For example, bimetallic catalysts have been shown to exhibit improvements over monometallic catalysts in various catalytic performance metrics for applications including petrochemical processing, ammonia synthesis, three-way catalysis, among many others.[5−16] While the idea of exploiting the properties of multiple catalytic materials to optimize performance is appealing, bimetallic catalyst design is complicated by the phase space of physical effects that control the relative geometries and organization of the constituent elements at the surface of bimetallic nanoparticles.

On the basis of the composition, mixing enthalpy, and size of bimetallic particles, various bulk structures can form, including solid solutions, ideal solutions, intermetallic compounds, and biphasic compounds.[1] It is also known that the composition and compositional ordering at bimetallic surfaces may vary from the bulk due to differences in surface energies of the metals.[17] For example, the lower surface free energy of noble metals (e.g., Pd, Pt, and Au) as compared to that of base metals (e.g., Fe, Co, Cu, and Ni) has been demonstrated to induce

Received: October 4, 2017
Revised: November 29, 2017
Published: December 5, 2017

DOI: 10.1021/acssuschemeng.7b03572
ACS Sustainable Chem. Eng. XXXX, XXX, XXX−XXX

surface enrichment of the noble metals, forming structures known as near surface alloys.[17,18] In addition to inherent interactions between the metals controlling the exposed surface structure and composition, it has also been shown that adsorbates can drive segregation of metals in bimetallic particles based on preferential interactions with one of the metals.[19−21] The demonstrated importance of bimetallic supported catalysts, combined with the inherent complexity associated with structure and reactivity of these catalytic materials, has motivated efforts to develop approaches that allow control of bimetallic surface structures and reactivity in predictable fashions.[18,22,23]

The conversion of biomass-derived molecules into fuels and chemicals provides a potentially viable alternative to petroleum-based fuels and chemicals,[24] although catalysts that exhibit excellent specificity in the conversion of multifunctional molecules are required to achieve economically viable process yields. Furfural (FF) is a renewable platform chemical that can be produced at high yields from pentose sugars by acid hydrolysis of lignocellulosic biomass.[24,25] Hydrodeoxygenation (HDO) of FF to produce methyl furan (MF) has gained interest due to the potential use of MF as an octane booster to gasoline, or as a precursor for diesel or jet fuel range branched alkanes.[26−28] Achieving high yields in FF conversion to MF requires catalysts that readily dissociate H_2 to enable hydrogenolysis of the aldehyde moiety and have concurrent specificity to interact with the aldehyde moiety rather than coordination to the furan ring to minimize unwanted decarbonylation, ring hydrogenation, and ring opening.[29−37] Achieving this reactivity and specificity requires development of bifunctional catalysts, as monometallic surfaces that enable facile H_2 dissociation (e.g., Pt, Pd, Ni, etc.) also preferentially coordinate the furan ring, while metal surfaces that selectively interact with the aldehyde (e.g., Cu or Ag) exhibit relatively low rates of H_2 dissociation.

Various strategies have been developed to achieve this type of catalytic behavior. For example, single atom alloys with noble metals atoms, such as Pt or Pd, dispersed on Cu surfaces enable H_2 dissociation at the noble metal active site and spillover of atomic H onto the Cu surface such that the catalyst can readily dissociate H_2 while exploiting the inherent catalytic properties of Cu surfaces.[38] A critical consideration in the design of these materials is whether the relative stoichiometry and organization of the two metal components will remain optimal at the catalytic surface over the catalyst lifetime. For the case of Cu−Ni bimetallic catalytic particles supported on TiO_2, we recently demonstrated that support-induced bimetallic particle segregation occurred where Ni preferentially localized at the TiO_2 interface and Cu preferentially localized at the bimetallic particle surface.[39] The existence of a low relative concentration of Ni at the catalytic surface allowed for enhanced rates of FF conversion to MF, as compared to a pure Cu catalyst, while maintaining selectivity typical of pure Cu catalysts. In addition, it was observed that having Ni segregated to the TiO_2 interface promoted catalytic stability against particle sintering. These results are promising in terms of the development of low cost, stable, and efficient catalysts for FF conversion to MF. However, because the previous report only considered a single bimetallic composition, a more thorough analysis of the influence of composition on reactivity and stability is required for performance optimization.

Here, we report a detailed analysis of Cu−Ni bimetallic catalysts, relating the influence of metal (with variation in Ni weight loading of 0−10 wt %, at a constant Cu loading of 5 wt %) and support composition (comparing TiO_2 and Al_2O_3) to metal particle structure, catalytic reactivity for FF HDO, and catalyst stability. It was observed via depth profiling X-ray photoelectron spectroscopy (DP-XPS) analysis that across a broad range of Ni weight loadings consistent distributions of Cu and Ni were present throughout bimetallic particles when Al_2O_3 was used as a support, whereas when TiO_2 was used as a support, the bimetallic particle surface was enriched in Cu as compared to the bulk composition. The addition of Ni to Cu(5 wt %)/Al_2O_3 catalysts, even at a low 0.5 wt %, resulted in FF ring hydrogenation and reduced MF yields. In contrast, the addition of Ni to Cu/TiO_2 at 0−5 wt % promoted FF HDO reactivity while maintaining high MF yields (∼85−90%), although the addition of Ni at >5 wt % resulted in reduced MF yields due to ring hydrogenation of MF. Both the stability and the regenerability of the Cu/TiO_2 catalyst were promoted by the addition of Ni at all tested weight loadings (0−5%), showing quantitative regenerability of the catalytic behavior of the as-synthesized material. This work demonstrates that by controlling metal composition and importantly metal−support interactions in Cu−Ni bimetallic catalysts, catalytic activity, selectivity, and stability for FF conversion to MF can be optimized. We expect that this approach for controlling the surface composition of bimetallic particles will be broadly applicable to catalytic systems that require a balance of reactivity and selectivity.

MATERIALS AND METHODS

Synthesis of Monometallic Cu Catalysts. In a typical synthesis, copper(II) nitrate trihydrate ($Cu(NO_3)_2{\cdot}3H_2O$, purity 99%, CAS: 10031-43-3, Aldrich, NJ) was dissolved in 50 mL of deionized (DI) water and added to 5 g of θ-Al_2O_3 (catalog no: 26R-0804UPG, Inframat Advanced Materials, Manchester, CT) or TiO_2 (P25, batch no. 4161060398, NIPPON AEROSIL Co., Ltd., Evonik, Degussa GmbH) contained in a round-bottom flask to obtain a 5 wt % loading of Cu. The solution was mixed and dried at 80 °C in a rotary evaporator. The resulting solids were dried at 100 °C for 12 h in an oven and calcined at 450 °C for 5 h in air. Prior to reactivity experiments, catalysts were reduced by pure H_2 at a flow rate of 50 mL min^{-1} at 450 °C for 3 h and cooled to 25 °C under the same environment.

Synthesis of Bimetallic Cu(5 wt %)−Ni(0.5, 1.5, 3, 5, and 10 wt %) Catalysts. Catalysts were prepared by adding the required amounts of $Cu(NO_3)_2{\cdot}3H_2O$ and $Ni(NO_3)_2{\cdot}6H_2O$ (Aldrich, purity 99.99%, St. Louis, MO) precursors simultaneously to achieve 5 wt % of Cu and 0.5, 1.5, 3, 5, and 10 wt % of Ni in 50 mL of DI water. This solution was added to 5 g of TiO_2 (P25) or θ-Al_2O_3 in a round-bottom flask. It was thoroughly mixed and dried at 80 °C using a rotary evaporator. The obtained material was dried in a vacuum oven at 100 °C for 12 h followed by calcination at 450 °C for 5 h. Prior to reactivity experiments, catalysts were reduced by pure H_2 at a flow rate of 50 mL min^{-1} at 450 °C for 3 h and cooled to 25 °C under the same environment.

Catalyst Characterization. *Transmission Electron Microscopy (TEM).* Transmission electron microscope (TEM) images were obtained using a FEI-Tecnai 12 TEM operating at an accelerating voltage of 120 kV.

X-ray Photoelectron Spectroscopy (XPS). XPS experiments were carried out using a Kratos AXIS ULTRADLD XPS system equipped with an Al Kα monochromated X-ray source and a 165 mm mean radius electron energy hemispherical analyzer. Vacuum pressure was kept below 3×10^{-9} Torr during analysis. Binding energy calibrations were done with reference to the carbon 1s peak by adjusting spectra to 284.8 eV. Depth profiling experiments were conducted by argon sputtering samples for 0, 1, 5, 10, 30, and 60 min with a beam voltage of 4 kV, current of 2.35 A, spot size of 3×3 mm^2, and vacuum

DOI: 10.1021/acssuschemeng.7b03572
ACS Sustainable Chem. Eng. XXXX, XXX, XXX−XXX

pressure of 3×10^{-9} Torr during acquisition. The surface composition of bimetallic Cu/Ni catalysts was calculated using sensitivity factors of 5.321 and 4.044 for Cu and Ni, respectively.

X-ray Diffraction (XRD). XRD spectra of reduced Cu(5%) and Cu(5%)−Ni(3%) on TiO_2 and Al_2O_3 catalysts were recorded in the 2θ range of 20−90° using an X'pert Pro PANalytical diffractometer equipped with a nickel filtered Cu Kα radiation source.

Dispersion Measurements. Chemisorption studies were carried out on a Micromeritics AutoChem 2920 instrument. In each experiment, 0.1 g of catalyst was placed in a U-tube quartz funnel and purged with Ar gas at 50 mL min^{-1} at 100 °C for 1 h. A gas mixture of H_2 (10%)/Ar was passed through the quartz funnel at 25 °C for 1 h with a 50 mL min^{-1} flow rate. The temperature was raised to 350 °C at a heating rate of 10 °C min^{-1}, and then the temperature was reduced to 50 °C under Ar (50 mL min^{-1}) for chemisorption studies. At 50 °C, catalysts were treated with 1000 ppm of N_2O/He with a 30 mL min^{-1} flow rate for 1 h followed by purging with Ar flow (50 mL min^{-1}) for 1 h at constant remperature. The temperature then was raised to 350 °C at a heating rate of 10 °C min^{-1} with 50 mL min^{-1} flow of H_2(10%)/Ar gas, and the amount of H_2 consumption was measured. Repeated N_2O oxidation followed by H_2-TPR experiments were conducted, and the average hydrogen consumption of four sequential experiments was used to calculate dispersion by using a 2:1 Cu/H_2 ratio.

Reactivity Measurements. Prior to each reaction, Cu and Cu−Ni catalysts were reduced at 450 °C for 3 h. Without exposure to air, 0.3 g of reduced catalysts was transferred into a 100 mL stainless-steel Parr micro benchtop reactor (4590 Series, Parr instruments Co., Moline, IL) containing 1 g of FF (99.9% pure, Sigma-Aldrich) with 25 mL of 1,4-dioxane (HPLC grade, Fisher Chemicals) as a solvent. The reactor was initially flushed with H_2 and then pressurized with H_2 gas. Next, the reactor temperature was raised to 200 °C, and reactions were conducted for 0.5−8 h.

Product Analysis. Liquid products were analyzed on an Agilent gas chromatograph (7890A, Agilent Technologies). A DB-WAX Ultra Inert column (Agilent Technologies) that was 30 m long × 0.320 mm internal diameter × 0.5 μm was used to quantify FF, furfuryl alcohol (FOL), and tetrahydrofurfuryl alcohol (THFOL) using a flame ionization detector (FID) during the following program: hold for 1 min at 30 °C, increase from 30 to 100 °C at a ramp rate of 10 °C min^{-1}, hold for 2 min at 100 °C, increase from 100 to 250 °C at a ramp rate of 10 °C min^{-1}. MF and methyl tetrahydrofuran (MTHF) were analyzed using an Hp-5 column that was 30 m long × 0.320 mm internal diameter × 0.25 μm via FID using the following program: 1 min hold at 30 °C, increase from 30−100 °C at a ramp rate of 10 °C/min, 2 min hold, increase from 100−325 °C at a ramp rate of 25 °C/min, and hold for 1 min. Molar yields of the final product were quantified by using calibration curves of standard samples in the gas chromatograph. Mass balances accounting for >95% of the carbon content were obtained in all experiments. Reactant conversion and product yield were calculated as follows:

$$\text{FF conversion\%} = \left(1 - \frac{\text{moles of unreacted FF}}{\text{moles of FF before reaction}}\right) \times 100 \quad (1)$$

$$\text{yields (mol \%)} = \frac{\text{moles of the product formed}}{\text{initial mole of FF}} \times 100 \quad (2)$$

Catalyst Recyclability. 0.3 g of freshly reduced catalyst was transferred into a 100 mL stainless-steel Parr reactor containing 1 g of FF and 25 mL of 1,4-dioxane. The reactor was flushed with H_2 and then pressurized with H_2 to 35 bar. Each reaction was conducted for 2 h at 200 °C. After completion of the reaction, the reactor was cooled by quickly lowering it into a room temperature water bath (25 °C) and depressurizing in the fume hood. The catalyst then was separated from the liquid by filtration and dried at 105 °C for 3 h and then reused in four recycle experiments without washing (or) regeneration. Regeneration of the used catalysts was performed via calcination at 450 °C for 5 h followed by reduction with pure H_2 at 450 °C for 3 h.

RESULTS

Catalyst Characterization. A series of catalysts with varied Ni loading and support were synthesized, consisting of Cu(5 wt %)−Ni(0, 0.5, 1.5, 3, 5, and 10 wt %)/TiO_2 and Cu(5 wt %)−Ni(0, 0.5, 1.5, 3, and 5 wt %)/Al_2O_3. Prior examination of Cu(5 wt %)−Ni(5 wt %) catalysts on TiO_2 and Al_2O_3 with TEM-based energy dispersive spectroscopy revealed that all observed metal particles contained both Cu and Ni, suggesting consistent formation of bimetallic particles.[39] The analysis was consistent with characterization using temperature-programmed reduction and X-ray diffraction, which both showed evidence of the formation of bimetallic particles. On the basis of this previous analysis, we focused here on analyzing the influence of Ni loading on the structure (both geometric and spatially varying composition) of the Cu−Ni bimetallic particles. Representative TEM images of Cu(5 wt %)−Ni(X wt %)/TiO_2 catalysts with Ni loadings of 0.5, 1.5, and 3.0 wt % are shown in Figure 1a−c.

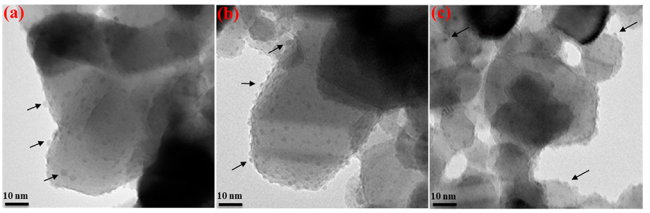

Figure 1. Representative TEM images of bimetallic Cu−Ni/TiO_2 catalysts: (a) Cu(5%)−Ni(0.5%)/TiO_2, (b) Cu(5%)−Ni(1.5%)/TiO_2, and (c) Cu(5%)−Ni(3%)/TiO_2. The black arrows point to bimetallic Cu−Ni particles.

The average Cu−Ni particle diameter, standard deviation, and size distribution (Figure S1) were measured by characterizing >100 particles from the corresponding TEM images of each sample. The average Cu−Ni particle size was statistically similar in these three representative materials: Cu(5 wt %)−Ni(0.5 wt %) ≈ 3.3 ± 0.7 nm > Cu(5 wt %)−Ni(1.5 wt %) ≈ 3.1 ± 0.8 nm > Cu(5 wt %)−Ni(3 wt %) ≈ 3.0 ± 1.0 nm. The particle size distributions were relatively tight in all cases examined, with only a few metallic particles with diameters >5 nm for the catalysts containing 1.5 and 3 wt % Ni. The particle sizes are in reasonable agreement with dispersions of 15.9% and 27.1% that give estimated average Cu particle diameters of 6.3 and 3.8 nm measured by N_2O titration for Cu(5%)/TiO_2 and Cu(5%)/Al_2O_3, respectively. Given our previous conclusion that observed support effects on FF HDO reaction selectivity were not significantly influenced by differences in metal particle size of the same magnitude of variation observed here, we focused on analyzing the spatial distribution of Cu and Ni in bimetallic particles as a function of metal and support composition.[39] We note that differences in metal particle sizes as a function of support influenced the inherent reactivity of the catalysts.

To analyze the spatial distribution of Cu and Ni in the bimetallic particles of varying composition on Al_2O_3 and TiO_2 supports, DP-XPS spectra were collected for the Cu−Ni catalysts as a function of Ar ion sputtering time. Because these are supported catalysts, relationships between sputtering time and sputtering depth are difficult to interpret. Thus, the data are simply reported as a function of Ar sputtering time, which is assumed to be proportional to depth into the Cu−Ni particles. The relative Cu and Ni concentrations were calculated by summing all contributions to the Cu 2p3/2 and Ni 2p3/2 peaks

DOI: 10.1021/acssuschemeng.7b03572
ACS Sustainable Chem. Eng. XXXX, XXX, XXX−XXX

and normalizing by their relative cross sections (sensitivity factors).[39]

Binding energy values for the Cu^0 and Ni^0 components of the 2p3/2 peaks were in the range of 931.8−932.3 and 851.8−852.9 eV, respectively, consistent with values reported in the literature.[37,40,41] Increasing the Ni loading from 1.5% to 5% increased the binding energy for the Ni^0 2p3/2 peak by ∼0.4−0.5 eV for both the TiO_2 and the Al_2O_3 supports (Table S1). However, when TiO_2 was used as a support, the Cu^0 2p3/2 peak position shifted up in binding energy by ∼0.5 eV as the Ni loading increased, while the Cu^0 2p3/2 peak position stayed essentially constant as Ni loading was varied on the Al_2O_3 supported catalysts. These results suggest that when Al_2O_3 was used as a support, Ni had minimal influence on the electronic environment of Cu, whereas when TiO_2 was used as a support, Ni addition significantly modified the local environment of Cu.

The DP-XPS composition profiles for Cu(5%)−Ni(1.5%, 3%, and 5%) on TiO_2 and Al_2O_3 are shown in Figure 2, with the corresponding spectra in Figures S2−S7. In each case, Ar sputtering was applied for ∼60 min, as we found that this was sufficient for the relative Cu and Ni concentrations to converge toward a bulk value. Figure 2a shows the DP-XPS profiles for Cu(5%)−Ni(1.5%) on TiO_2 and Al_2O_3, plotted in terms of the relative percent of Cu and Ni at each sputtering time. Given the nominal weight loadings, a Cu:Ni ratio of 77%:23% would be expected if the metals were evenly distributed throughout the bimetallic particles. For the Al_2O_3 support, an almost constant 72−76% nominal Cu % was observed at Ar sputtering times between 0 and 30 min, with a slight increase to ∼81% Cu at 60 min Ar sputtering. This result suggests that the Cu and Ni were distributed virtually homogeneously in the samples at close to the nominally expected relative concentrations. However, for the TiO_2 supported catalyst, an 88% Cu relative concentration was measured prior to Ar sputtering and then steadily converged toward 82% at 60 min of Ar sputtering time.

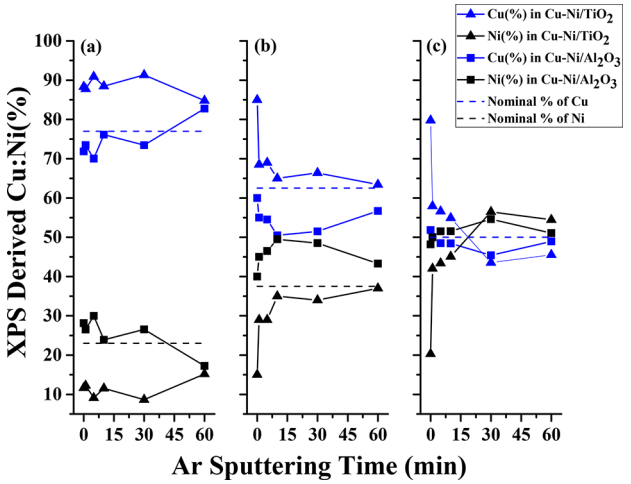

Figure 2. Relative Cu and Ni concentrations derived from deconvolution of the DP-XPS spectra as a function of argon sputtering time where (a), (b), and (c) show the data for Cu(5%)−Ni(0.5%)/TiO_2 and Al_2O_3, Cu(5%)−Ni(3%)/TiO_2 and Al_2O_3, and Cu(5%)−Ni(5%)/TiO_2 and Al_2O_3 catalysts, respectively. The data in Figure 2c are adapted from ref 39. The relative Ni concentrations are shown in black, and Cu concentrations are shown in blue. Data for Al_2O_3 supported catalysts are depicted in squares, whereas TiO_2 are in triangles. The dotted lines are the expected Ni and Cu concentrations based on nominal bulk compositions.

The Cu(5%)−Ni(3%) and Cu(5%)−Ni(5%) catalysts showed behavior similar to that of the Cu(5%)−Ni(1.5%) catalysts, where the Cu concentration was enhanced at the bimetallic particle surfaces as compared to the bulk for a TiO_2 support, Figure 2b,c. For the Cu(5%)−Ni(3%) catalyst, the relative Cu surface concentration (Ar sputtering time = 0) was ∼25% greater when TiO_2 was used as a support as compared to Al_2O_3 (85% for TiO_2 versus 60% for Al_2O_3), whereas this difference increased to 30% for the Cu(5%)−Ni(5%) catalyst (80% for TiO_2 versus 50% for Al_2O_3). In addition, for the Cu(5%)−Ni(3%) and Cu(5%)−Ni(5%) catalyst, as the Ar sputtering time increased to 60 min, the Cu and Ni relative concentrations converged toward the expected nominal loadings for the TiO_2 supported catalysts. In contrast, the Cu and Ni relative concentrations varied only slightly as a function of Ar sputtering time and from the expected nominal concentrations when Al_2O_3 was used as a support.

In all analyzed cases, we observed evidence of a significant influence of the support on the composition structure of the bimetallic Cu−Ni particles, where when TiO_2 was used as a support Cu was enriched at the catalyst surface, while on Al_2O_3, Cu and Ni were present in close to the nominal concentration throughout the catalyst particles. Comparing the TiO_2 supported catalysts, the Cu surface loading (at Ar sputtering time = 0) decreased from 88% to 80% as the Ni loading increased from 1.5% to 5%. However, for the Al_2O_3 supported catalysts, the Cu surface loading varied more significantly, from 72% to 51% as Ni loading was increased, which is consistent with the expected decrease from 77% to 50% based on nominal metal loadings. From this analysis, it is clear that at all explored Ni loadings, TiO_2 induces Cu segregation to the bimetallic particle surfaces, while maintaining a small 10−20% Ni surface concentration.

Scheme 1. FF Hydrogenation Reaction Pathways[a]

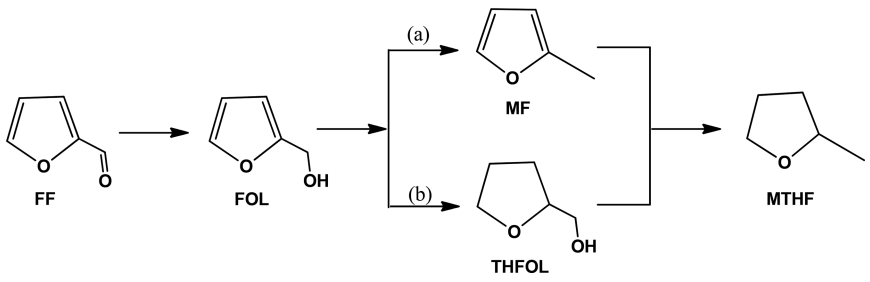

[a]Path (a) represents the hydrogenolysis of FOL to MF followed by ring hydrogenation of MF to form MTHF. Path (b) represents furan ring hydrogenation in FOL to form THFOL followed by further hydrogenolysis THFOL to form MTHF.

DOI: 10.1021/acssuschemeng.7b03572
ACS Sustainable Chem. Eng. XXXX, XXX, XXX−XXX

Catalytic Activity Studies. HDO of FF to MF occurs through sequential steps, where initial hydrogenation of the FF carbonyl group forms FOL and further hydrogenolysis of FOL produces MF, Scheme 1. An unwanted side product, THFOL, can form from ring hydrogenation of FOL and is commonly observed on catalysts that promote coordination with the furan ring. Another unwanted side product, MTHF, could form from either furan ring hydrogenation of MF, or hydrogenolysis of THFOL, Scheme 1. Thus, to maximize reactivity and selectivity for MF formation, a catalyst must be able to drive H_2 dissociation facilely, while minimizing coordination to the furan ring.[37,39,42,43]

To explore how the bimetallic Cu−Ni composition and support influence reactivity, selectivity, and stability in the FF HDO reaction, preliminary experiments were conducted over Cu(5%)−Ni(0.5, 1.5, and 3%)/TiO_2 catalysts at reaction times between 0.5 and 8 h, H_2 pressure between 25 and 45 bar, with 25 mL of 1,4-dioxane as a solvent, 30 wt % catalyst to FF loading, and a temperature of 200 °C. Figure S8 shows the FF conversion, MF yield, and FOL yield (the two major identified products) over Cu(5%)−Ni (0.5, 1.5, and 3%)/TiO_2 catalysts as a function of reaction time. FF conversion increased with reaction time, and MF was the major product for all catalysts. However, at 8 h reaction time, the total yields of identified products were between 50% and 75%, while greater than 85% FF conversion was observed for all catalysts. It is proposed that the unquantified products derived from FF degradation, which is known to occur when low loadings of catalysts with minimal ability for H_2 dissociation are used.[44,45] To overcome this, the influence of H_2 pressure was examined by measuring the FF HDO reaction at 25, 35, and 45 bar over the Cu(5%)−Ni(0.5%)/TiO_2 catalyst; see Table S2. At 35 bar H_2 pressure, MF yields increased to >90% at 100% FF conversions, and no further increase was seen at 45 bar H_2 pressure. Therefore, further studies comparing the influence of catalyst composition on FF HDO activity, selectivity, and stability were executed at 35 bar H_2 pressure, with all other conditions held constant.

Figure 3 shows FF conversion and product yields over monometallic Cu(5%) and bimetallic Cu(5%)−Ni(0.5, 1.5, and 3%)/Al_2O_3 catalysts as a function of reaction time. On

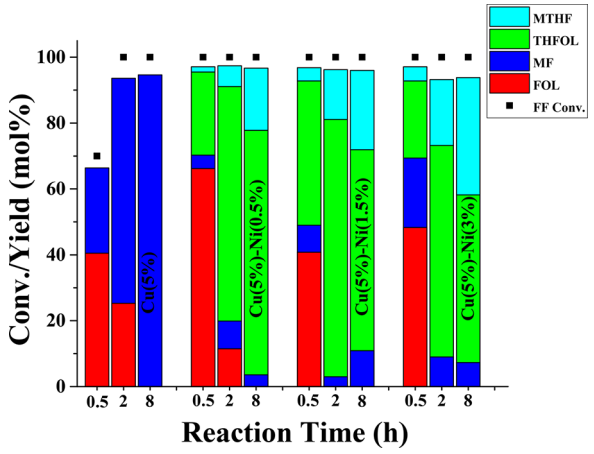

Figure 3. FF conversion and product yields as a function of reaction time on Cu/Al_2O_3 and Cu−Ni/Al_2O_3 catalysts. The catalyst composition is noted in the 8 h reaction time bar. All reactions were conducted at FF loading of 1 g, catalyst loading of 0.3 g, with 25 mL of 1,4-dioxane as a solvent, and at a temperature of 200 °C. The reactor was pressurized with 35 bar H_2 gas at 25 °C.

Cu(5%)/Al_2O_3, FF conversions were 70% and 100% at 0.5 and 2 h reaction time, respectively, and a maximum of 94.6% MF yield was obtained at 8 h reaction time. The addition of 0.5% Ni caused an increase in catalytic reactivity, where complete FF conversion was observed within 0.5 h. However, the dominant products were FOL and THFOL at all explored reaction times, with 74.2% and 18.9% yields of THFOL and MTHF observed, respectively, at 8 h reaction time.

The product distribution as a function of time was similar for the Cu(5%)−Ni(1.5 and 3%)/Al_2O_3 catalysts as compared to Cu(5%)−Ni(0.5%)/Al_2O_3, with THFOL and MTHF being the dominant products. Consistently across the Cu(5%)−Ni(0.5%, 1.5%, and 3%)/Al_2O_3 catalysts, it was observed that FOL was the most favored product at short times, followed by THFOL at intermediate times and increasing MTHF at longer times. Thus, for the Al_2O_3 supported bimetallic Cu−Ni catalysts, a dominant reaction pathway exists where FF is first hydrogenated to FOL, followed by ring hydrogenation to THFOL and finally hydrogenolysis to MTHF (Scheme 1, path b). Clearly, Ni enhanced the reactivity of the Cu/Al_2O_3 catalyst; however, the selectivity to MF was significantly diminished at all explored Ni loadings.

On the monometallic Cu(5%)/TiO_2 catalyst, FOL and MF were observed as the primary products, with a maximum MF yield of 53% and FF conversion of 91.5% at 8 h reaction time, Figure 4. As was observed for reactions run at lower H_2

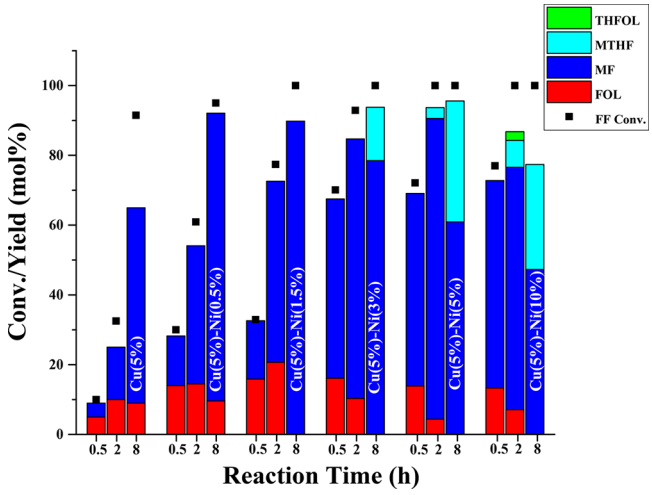

Figure 4. FF conversion and product yields as a function of time on Cu/TiO_2 and Cu−Ni/TiO_2 catalysts. The catalyst composition is noted in the 8 h reaction time bar. All reactions were conducted at FF loading of 1 g, catalyst loading of 0.3 g, with 25 mL of 1,4-dioxane as a solvent, and at a temperature of 200 °C. The reactor was pressurized with 35 bar H_2 gas at 25 °C.

pressures, Figure S8, the low rates of dissociative H_2 adsorption on the Cu(5%)/TiO_2 catalysts led to FF degradation instead of hydrogenation.[44,45] The observation of higher reactivity for monometallic Cu catalysts on Al_2O_3 as compared to TiO_2 is consistent with the differences in measured Cu dispersion for these catalysts of 27.1% for Cu(5%)/Al_2O_3 and 15.7% for Cu(5%)/TiO_2. Our previous study demonstrated that, apart from the difference in reactivity of Cu on Al_2O_3 and TiO_2, which can be explained by the differences in dispersion, differences in surface acidity of the support seemed to not contribute to differences in reactivity of the catalysts.[39] On the basis of this, any differences in FF HDO selectivity over Cu−Ni

DOI: 10.1021/acssuschemeng.7b03572
ACS Sustainable Chem. Eng. XXXX, XXX, XXX−XXX

catalysts on Al_2O_3 and TiO_2 are attributed strictly to differences in metal concentration and arrangements at the catalytic surface.

The influence of Ni addition to the supported Cu catalysts was observed to be different for the TiO_2 supported catalysts, as compared to the Al_2O_3 supported catalysts. The addition of 0.5 and 1.5% Ni loadings, to form bimetallic Cu−Ni catalysts on TiO_2, enhanced FF conversion and MF yields, as compared to the Cu(5%)/TiO_2 catalyst. FF conversion increased ∼3× on Cu(5%)−Ni(0.5% and 1.5%)/TiO_2 as compared to Cu(5%)/TiO_2 catalyst at 0.5 and 2 h reaction time. Furthermore, MF yield was enhanced due to the addition of 0.5% and 1.5% Ni, where at 8 h reaction time 83% and 90% MF yields were observed, respectively. When the Ni loading was further increased, to form Cu(5%)−Ni(3 and 5%)/TiO_2 catalysts, FF conversion at 0.5 h reaction time increased 2× as compared to the Cu(5%)−Ni(0.5 and 1.5)/TiO_2 catalysts. Maximum MF yields of 74.4% and 86.2% were observed at 2 h reaction time on Cu(5%)−Ni(3%)/TiO_2 and Cu(5%)−Ni(5%)/TiO_2 catalysts, respectively. MF yields were diminished at longer reaction times for the Cu(5%)−Ni(3 and 5%)/TiO_2 catalysts due to the formation of MTHF. Further increasing the Ni loadings to 10% showed minimal influence on the FF HDO reactivity as compared to lower Ni loadings, and diminished MF selectivity due to an increased rate of MTHF formation and the apparent degradation of FF or hydrogenation products.

Interestingly, as compared to the bimetallic Cu−Ni/Al_2O_3 catalysts where MTHF was formed through the hydrogenolysis of THFOL, the time-dependent reactivity measurements on bimetallic Cu−Ni/TiO_2 catalysts suggested that MTHF forms from ring hydrogenation of MF (Scheme 1, path a). To verify this, pure MF hydrogenation was executed over monometallic Cu(5%)/TiO_2 and bimetallic Cu(5%)−Ni(0.5 and 1.5%)/TiO_2 catalysts using 4 h reaction time, under conditions similar to those of the FF HDO experiments. As shown in Figure 5, essentially no conversion of MF was observed over the Cu(5%)/TiO_2 catalyst, which is consistent with the minimal expected interaction between the furan ring of MF and the pure Cu surface. On the Cu(5%)−Ni(0.5%)/TiO_2 and Cu(5%)−Ni(1.5%)/TiO_2 catalysts, 14.1% and 33.5% yields of MTHF were formed, respectively, with minimal side product formation. This demonstrates that Ni addition to Cu/TiO_2 catalysts promotes selective ring hydrogenation of MF to MTHF, and together with the time-dependent FF HDO reactivity of these catalysts suggests that MTHF forms on TiO_2 supported bimetallic Cu−Ni catalysts through ring hydrogenation of MF.

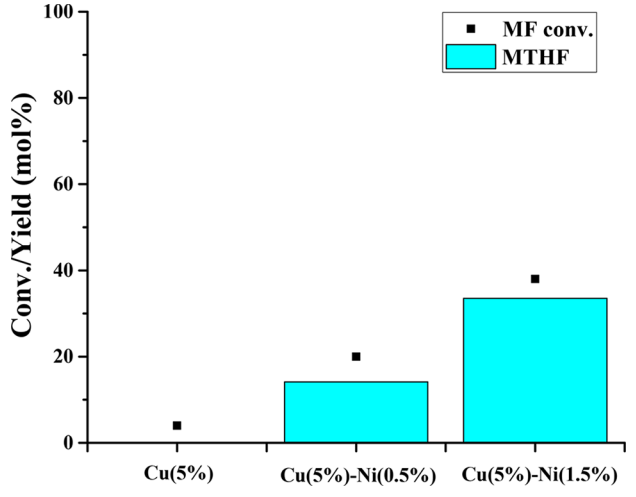

Figure 5. MF conversion and MTHF yield over Cu(5%)/TiO_2 and Cu(5%)−Ni(0.5 and 1.5%)/TiO_2 catalysts. Reactions were conducted at MF loading of 1 g, catalyst loading of 0.3 g, with 25 mL of 1, 4-dioxane as a solvent, temperature of 200 °C, 35 bar of H_2 (at 25 °C), and 4 h reaction time.

To summarize the reactivity results, it was observed for both Al_2O_3 and TiO_2 supported catalysts that the addition of only 0.5% Ni to Cu catalysts significantly promotes FF HDO reactivity, which is postulated to occur by enhanced rates of H_2 dissociation on exposed Ni sites. However, the addition of even a small amount of Ni (0.5%) to Cu(5%)/Al_2O_3 catalysts induced ring hydrogenation of FOL to form THFOL, rather than hydrogenolysis to produce MF. Alternatively, when TiO_2 was used as a support, even at 10% Ni loading, FOL hydrogenolysis to MF is the favored pathway over ring hydrogenation to form THFOL. As a result of this difference in behavior, the ultimate production of MTHF occurs through different reaction pathways when the Cu−Ni bimetallic catalyst is supported on TiO_2 or Al_2O_3, where on TiO_2 MF is the intermediate, while on Al_2O_3 THFOL is the intermediate.

The reactivity results suggest that MF yields on Cu(5%)−Ni(X%)/TiO_2 catalysts are optimized at 1.5−5% Ni loading depending on the reaction time. It is worth noting that the monometallic Cu/Al_2O_3 catalyst showed MF yields comparable to those of the optimized Cu−Ni/TiO_2 catalyst, although it has been shown previously that Cu/Al_2O_3 is unstable under FF HDO reaction conditions due to carbon deposition and Cu sintering.[39] To compare catalytic stability of the TiO_2 supported catalysts, recycle experiments were performed where catalysts were recycled sequentially for four reactivity experiments (R1−R4) followed by regeneration through calcination and reduction and a final reactivity test (R5). R1−R4 probe the change in catalytic reactivity due to carbon deposition and Cu sintering or leaching into solution, while R5 allows analysis of only the influence of Cu sintering or leaching as regeneration removes all carbon deposits. FF conversion was kept below 100% in all experiments.

Figure 6a shows that for the monometallic Cu(5%)/TiO_2 catalyst, FF conversion and MF yields decreased from 37.3% (in R1) to 25.5% (in R4) and 16.8% (R1) to 4.2% (R4), respectively, showing a significant loss of performance. Regeneration of the catalyst promoted the FF conversion and MF selectivity in R5 to an FF conversion and MF yield similar to those observed in R1. Figure 6b shows that the addition of 0.5% Ni to the Cu(5%)/TiO_2 catalyst improved the stability of the catalytic activity during R1−R4, with an essentially constant FF conversion of ∼61−68%, although the MF yield decreased from 37% to 11%. Following regeneration, the Cu(5%)−Ni(0.5%)/TiO_2 catalyst showed reactivity similar to that in R1, but with slightly decreased MF yields. Further increase in Ni loading continued to improve the stability of the catalysts. This behavior is most notable for the Cu(5%)−Ni(5%)/TiO_2 catalyst in Figure 6d, where FF conversion decreased only slightly from 99% to 88% from R1 to R4, and MF yields decreased from 87% to 60% comparing R1−R4. Similar to the other catalyst, the behavior of the Cu(5%)−Ni(5%)/TiO_2 following regeneration, R5, was almost identical to R1 with 87% MF yields.

The recycle and regeneration results in Figure 6 demonstrated that the Cu(5%)/TiO_2 catalyst stability, in terms of

DOI: 10.1021/acssuschemeng.7b03572
ACS Sustainable Chem. Eng. XXXX, XXX, XXX−XXX

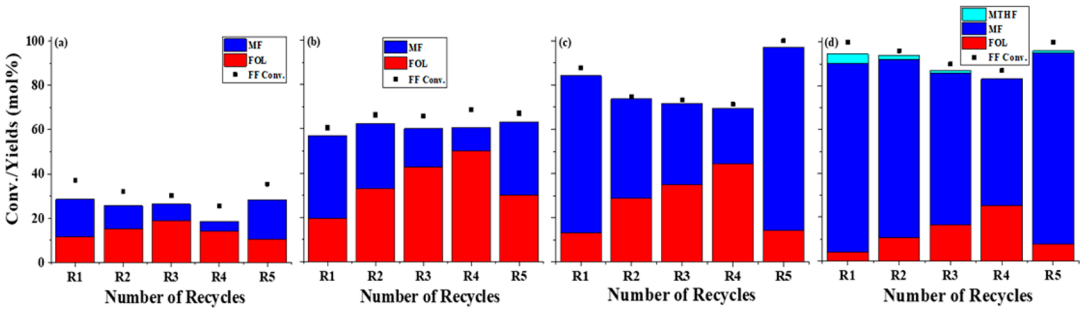

Figure 6. FF conversion and product yields as a function of recycles, R, for (a) Cu(5%)/TiO_2, (b) Cu(5%)−Ni(0.5%)/TiO_2,(c) Cu(5%)−Ni(3%)/TiO_2, and (d) Cu(5%)−Ni(5%)/TiO_2 catalysts. Prior to regeneration (before R5), each catalyst was calcined at 450 °C for 5 h and reduced at 450 °C for 3 h under H_2 flow (50 mL/min). Reaction conditions were a FF loading of 1 g, catalyst loading of 0.3 g, with 25 mL of 1,4-dioxane as solvent, temperature of 200 °C, H_2 pressure of 35 bar (at 25 °C), and 2 h reaction time.

activity, selectivity, and regenerability, are all promoted by Ni addition, and that catalyst stability is optimized at the highest Ni loadings. It is also important to point out that in the bimetallic Cu−Ni/TiO_2 catalysts, throughout the explored recycle and regeneration, the catalyst retained a preference to drive first FF hydrogenation to FOL followed by FOL hydrogenolysis to MF, which is in stark contrast to the Cu−Ni/Al_2O_3 catalyst. Thus, by optimizing Cu−Ni bimetallic concentration, support composition, and reaction time, the activity, MF selectivity, and catalytic stability could be optimized.

DISCUSSION

We start by discussing evidence for how the composition of the support influences the structure of bimetallic Cu−Ni nanoparticles. In our previous work for Cu(5%)−Ni(5%) catalysts, a significant Cu surface segregation within the bimetallic particles was observed when TiO_2 was used as a support, whereas a homogeneous distribution of the metals throughout the bimetallic particles was observed when Al_2O_3 was used a support.[39] It was argued that this result was due to strong, specific interactions between Ni and TiO_2 that induced Ni segregation to the TiO_2 interface and Cu to the catalytic surface to minimize the energy of the supported particle. In contrast, the relatively similar interaction energy between Cu or Ni and Al_2O_3 caused the formation of bimetallic particles with homogeneous Ni and Cu distributions to be energetically favorably. We note that on both supports, enough Ni still existed at the bimetallic particle surfaces to significantly promote hydrogenation reactivity over the monometallic Cu catalysts. However, the amount of Ni at the surface controlled reactivity selectivity. The studies presented here extended insights to include understanding how support-induced segregation is influenced by Ni weight loading and postulating how Cu and Ni are spatially organized (relative to each other) at the bimetallic nanoparticle surfaces.

Figure 2 shows that, regardless of the Ni loading considered (1.5%, 3%, and 5%), the composition of Cu at the bimetallic particles surfaces is greater than 80% when TiO_2 was used as a support. However, in the case of 3% and 5% Ni loadings, the relative Cu concentration dropped significantly in the first few cycles of Ar sputtering. This result suggests that for TiO_2 supported Cu−Ni bimetallic catalysts, a relatively thin near-surface alloy is enriched in Cu, and that this behavior is consistent across various Ni loadings. Although DP-XPS analysis was not applied to the Cu(5%)−Ni(10%)/TiO_2 catalyst, dominant MF and FOL production at short reaction times and a lack of THFOL formation at longer times, as typically seen for monometallic Ni catalysts, strongly suggest that the near surface region is still enriched in Cu even when bulk Ni concentrations are twice that of Cu. The Cu surface segregation for bimetallic Cu−Ni catalysts on TiO_2 as measured by both DP-XPS and reactivity is in stark contrast with observations for the Al_2O_3 supported catalysts. It is well-known that catalyst pretreatment and exposure to reaction conditions can modify the structure of bimetallic particles.[46−50] However, the consistent evidence of support-induced Cu surface segregation observed here suggests that the influence of the support in controlling the compositional structure of the bimetallic particles is stronger than the influence of the pretreatment or reaction conditions on the structures. These results also suggest that the TiO_2-induced driving force for Cu surface segregation in bimetallic Cu−Ni particles is quite strong, even inducing this behavior when the Ni content is twice that of Cu.

In addition to the strong support-induced surface segregation of Cu in bimetallic Cu−Ni particles, combined DP-XPS and reactivity analysis also provides evidence of Cu and Ni organization at the surface. XPS analysis of the binding energy of the Cu^0 2p3/2 states (see Table S1) demonstrates that when Al_2O_3 is used as a support, the electronic environment of Cu is not significantly modified by increasing Ni loadings (the binding energy of Cu^0 2p3/2 is essentially constant). However, when TiO_2 is used as a support, the Cu^0 2p3/2 states shift up in energy by ∼0.5 eV as the Ni loading was increased from 1.5% to 5%. This suggests that when Al_2O_3 is used as a support the interactions between Cu and Ni are relatively small within the bimetallic particles, whereas there is significant charge transfer between Cu and Ni when TiO_2 is used as support. Another interesting observation is that when Al_2O_3 is used as support, Ni exists in a more oxidized state (a large fraction of Ni is not metallic) on the bimetallic particle surfaces, at a given Ni weight loading, as compared to TiO_2 as a support. Furthermore, in the DP-XPS experiments, it was observed that the existence of oxidized Ni persisted deeper into the Al_2O_3 supported bimetallic particles as compared to the TiO_2 supported particles. Taken together, we propose that Ni at the surface of Al_2O_3 supported bimetallic Cu−Ni particles exists in contiguous domains that have minimal interaction with Cu and can be easily oxidized, as shown in Scheme 2. Alternatively, it is suggested that Ni at the surface of Cu−Ni/TiO_2 catalysts is relatively scarce as compared to the same Ni content in Cu−Ni/Al_2O_3 catalysts, and that the dispersion of Ni within Cu

DOI: 10.1021/acssuschemeng.7b03572
ACS Sustainable Chem. Eng. XXXX, XXX, XXX−XXX

Scheme 2. Schematic Diagram of the Proposed Surface Composition and Structure of Bimetallic Particles Cu−Ni on Al_2O_3 and TiO_2 Supports for Cu(5%)−Ni(3%)[a]

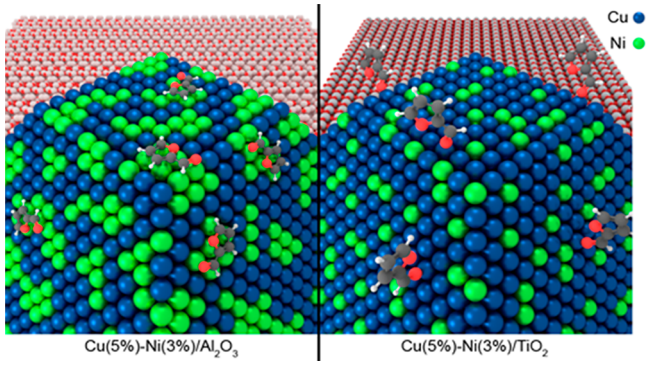

[a]In the case of Cu(5%)−Ni(3%)/Al_2O_3, significant contiguous surface Ni domains enabled more facile oxidation of the Ni and preferred FF adsorption through furan ring coordination. Alternatively, for Cu(5%)−Ni(3%)/TiO_2 catalysts, the catalyst surface is rich with Cu, containing mostly dispersed Ni species, which favored FF adsorption through carbonyl coordination.

induces significant charge transfer between the metals and reduces the propensity for Ni oxidization.

The proposed structures based on DP-XPS measurements are further supported by XRD analyses of Cu(5%) and Cu(5%)−Ni(3%) catalysts on TiO_2 and Al_2O_3, as shown in Figure S9. XRD spectra of Cu(5%)/TiO_2 and Cu(5%)/Al_2O_3 show sharp peaks at 43.7° and 43.9°, respectively, which correspond to the metallic Cu(111) reflection. The XRD spectrum in the same region for Cu(5%)−Ni(3%)/TiO_2 shows two diffraction peaks at 43.9° and 44.6°. The 43.9° diffraction peak is assigned to the surface alloy phase where the low Ni concentration existing as dispersed species only slightly expands the Cu lattice, while the 44.6° reflection is assigned to the Cu−Ni alloy phase existing in the bulk of the bimetallic particles. The results agree well with the DP-XPS data, which suggest two different phases of Cu−Ni alloys. Conversely, for Cu(5%)−Ni(3%)/Al_2O_3, the Cu(111) peak position shifted to >0.2° higher 2θ value as compared to Cu(5%)/Al_2O_3, suggesting that Cu exists in predominantly Cu domains within the bimetallic Cu−Ni particles. In both of the bimetallic catalysts, it was difficult to identify peaks associated with metallic Ni due to the lower loadings compared with Cu metal. The XRD analysis agreed well with the DP-XPS analysis, suggesting that on TiO_2, bimetallic Cu−Ni particles form a surface segregated domain with low Ni content, while on Al_2O_3, bimetallic Cu−Ni particles exist with a higher Ni content at the catalyst surface as compared to on TiO_2 and segregated Ni and Cu domains within the particles.

Reactivity studies provided further evidence for the proposed support-induced differences in organization of Cu and Ni at the bimetallic surfaces. For TiO_2 supported catalysts, there is no evidence of contiguous Ni surface domains at any considered Ni loadings. Ni is known to selectively coordinate to the furan ring in FF or FOL, rather than the carbonyl or alcohol groups. However, at even up to 10% Ni loadings, preferential alcohol hydrogenolysis was observed over ring hydrogenation, evidenced by MF selectivity rather than THFOL in Figure 4, suggesting that Ni exists at the bimetallic Cu−Ni/TiO_2 surface as dispersed species that cannot coordinate to the furan ring. For the Cu(5%)−Ni(10%)/TiO_2 catalyst, ring hydrogenation of MF to form MTHF was observed, but because THFOL was a product, it is evident that alcohol hydrogenolysis was favored over ring hydrogenation even at the highest Ni loadings when TiO_2 was used as a support. While these dispersed Ni surface species on Cu−Ni/TiO_2 catalysts had no preferential interaction with the furan ring over the alcohol group, the increased catalytic reactivity when Ni was added strongly suggests that the dispersed Ni species could still facilitate H_2 dissociation. Alternatively, at all considered Ni loadings on the Cu−Ni/Al_2O_3 catalysts, significant evidence for preferential furan ring coordination over alcohol coordination was postulated on the basis of the minimal MF yield and the preferential formation of THFOL. Furan ring coordination that is known to occur at Ni surfaces but not at Cu surfaces strongly suggests that Ni exists in contiguous domains on the nanoparticle surface of Cu−Ni/Al_2O_3 catalysts.

CONCLUSIONS

This work demonstrates that controlling metal composition and metal−support interactions in Cu−Ni bimetallic catalysts can simultaneously promote catalytic activity, selectivity, and stability for FF conversion to MF, as compared to monometallic Cu catalysts. Detailed analysis of Cu−Ni bimetallic particles on TiO_2 and Al_2O_3 supports suggests that over a range of bimetallic compositions, TiO_2 promotes formation of near surface alloys rich in Cu that primarily contain dispersed Ni species. Alternatively, when Cu−Ni bimetallic particles are synthesized on Al_2O_3 supports, evidence suggests that Cu and Ni are evenly distributed throughout the particles and there exists segregation of Ni and Cu domains at the particle surfaces. As a result of the support-induced changes in compositional structure of the bimetallic Cu−Ni particle surfaces, FF HDO results primarily in MF formation when TiO_2 is used as a support, while FOL and THFOL are the primary products when Al_2O_3 is used as a support. These results suggest that control of the surface structure and composition of bimetallic catalysts by choice of supports may be a generally useful strategy to influence reaction results for a range of catalytic processes.

ASSOCIATED CONTENT

Supporting Information

The Supporting Information is available free of charge on the ACS Publications website at DOI: 10.1021/acssuschemeng.7b03572.

Particle size distributions, XPS spectra and analysis, XRD spectra, and reactivity data provided in Figures S1−S9 and Tables S1 and S2 (PDF)

AUTHOR INFORMATION

Corresponding Author

*E-mail: christopher@engr.ucr.edu.

ORCID

Phillip Christopher: 0000-0002-4898-5510

Notes

The authors declare no competing financial interest.

ACKNOWLEDGMENTS

We acknowledge funding support from DOE-EERE BETO Office through award DE-EE0007006. Dr. Ilkeun Lee is acknowledged for assistance with the XPS analysis made

DOI: 10.1021/acssuschemeng.7b03572
ACS Sustainable Chem. Eng. XXXX, XXX, XXX−XXX

possible by NSF grant DMR-0958796. Dr. Kun Li is acknowledged for assistance in obtaining TEM images. TEM was carried out at UCR Central Facility for Advanced Microscopy and Microanalysis (CFAMM). Sergei Hanukovich is acknowledged for assistance in obtaining dispersion measurements.

REFERENCES

(1) Ponec, V. Alloy catalysts: The concepts. *Appl. Catal., A* **2001**, *222* (1−2), 31−45.
(2) Clarke, J. K. A. Selectivity Catalysis Alloys. *Chem. Rev.* **1974**, *75* (3), 291−305.
(3) Gao, F.; Goodman, D. W. Pd-Au Bimetallic Catalysts: Understanding Alloy Effects from Planar Models and (supported) Nanoparticles. *Chem. Soc. Rev.* **2012**, *41* (24), 8009−8020.
(4) Yi, C. W.; Luo, K.; Wei, T.; Goodman, D. W. The Composition and Structure of Pd - Au Surfaces. *J. Phys. Chem. B* **2005**, *109* (39), 18535−18540.
(5) Vu, B. K.; Song, M. B.; Ahn, I. Y.; Suh, Y. W.; Suh, D. J.; Kim, W. Il; Koh, H. L.; Choi, Y. G.; Shin, E. W. Pt-Sn Alloy Phases and Coke Mobility over Pt-Sn/Al2O3 and Pt-Sn/ZnAl2O4 Catalysts for Propane Dehydrogenation. *Appl. Catal., A* **2011**, *400* (1−2), 25−33.
(6) Jossens, L. W.; Petersen, E. E. Fouling of a Platinum-Rhenium Reforming Catalyst Using Model Reforming Reactions. *J. Catal.* **1982**, *76* (2), 265−273.
(7) Rasser, J. C.; Beindorff, W. H.; Scholten, J. J. F. Characterization and Performance of Platinum-Iridium Reforming Catalysts. *J. Catal.* **1979**, *59* (2), 211−222.
(8) Antolini, E.; Salgado, J. R. C.; Gonzalez, E. R. The stability of Pt-M (M = first row transition metal) Alloy Catalysts and Its Effect on the Activity in Low Temperature Fuel Cells. A Literature Review and Tests on a Pt-Co Catalyst. *J. Power Sources* **2006**, *160* (2 SPEC. ISS.), 957−968.
(9) Oh, S. H.; Carpenter, J. E. Platinum-Rhodium Synergism in Three-Way Automotive Catalysts. *J. Catal.* **1986**, *98* (1), 178−190.
(10) Calderone, V. R.; Shiju, N. R.; Ferré, D. C.; Rothenberg, G. Bimetallic Catalysts for the Fischer−Tropsch Reaction. *Green Chem.* **2011**, *13* (8), 1950−1959.
(11) Nørskov, J. K.; Bligaard, T.; Logadottir, A.; Bahn, S.; Hansen, L. B.; Bollinger, M.; Bengaard, H.; Hammer, B.; Sljivancanin, Z.; Mavrikakis, M.; et al. Universality in Heterogeneous Catalysis. *J. Catal.* **2002**, *209* (2), 275−278.
(12) Michaelides, A.; Liu, Z. P.; Zhang, C. J.; Alavi, A.; King, D. A.; Hu, P. Identification of General Linear Relationships Between Activation Energies and Enthalpy Changes for Dissociation Reactions at Surfaces. *J. Am. Chem. Soc.* **2003**, *125* (13), 3704−3705.
(13) Kojima, Y.; Miyaoka, H. Nitrogen Dissociation via Reaction with Lithium Alloys. *Acs Omega* **2017**, *2* (3), 1081−1088.
(14) Nikolla, E.; Schwank, J.; Linic, S. Promotion of the Long-term Stability of Reforming Ni Catalysts by Surface Alloying. *J. Catal.* **2007**, *250* (1), 85−93.
(15) Holewinski, A.; Idrobo, J.-C.; Linic, S. High-Performance Ag−Co Alloy Catalysts for Electrochemical Oxygen Reduction. *Nat. Chem.* **2014**, *6* (9), 828−834.
(16) Xin, H.; Holewinski, A.; Linic, S. Predictive Structure reactivity Models for Rapid Screening of pt-Based Multimetallic Electrocatalysts for the Oxygen Reduction Reaction. *ACS Catal.* **2012**, *2* (1), 12−16.
(17) Ruban, A.; Skriver, H.; Nørskov, J. Surface Segregation Energies in Transition-Metal Alloys. *Phys. Rev. B: Condens. Matter Mater. Phys.* **1999**, *59* (24), 15990−16000.
(18) Greeley, J.; Mavrikakis, M. Alloy CatalystsDesigned from First Principles. *Nat. Mater.* **2004**, *3* (11), 810−815.
(19) Padama, A. A. B.; Villaos, R. A. B.; Albia, J. R.; Diño, W. A.; Nakanishi, H.; Kasai, H. CO-Induced Pd Segregation and the Effect of Subsurface Pd on CO Adsorption on CuPd Surfaces. *J. Phys.: Condens. Matter* **2017**, *29* (2), 25005.
(20) Yao, Y.; Goodman, D. W. In situ IR Spectroscopic studies of Ni Surface Segregation Induced by CO Adsorption on Cu-Ni/SiO2 Bimetallic Catalysts. *Phys. Chem. Chem. Phys.* **2014**, *16* (8), 3823−3829.
(21) Nerlov, J.; Chorkendorff, I. Promotion Through Gas phase Induced Surface Segregation: Methanol Synthesis from CO, CO2 and H2 Over Ni/Cu (100). *Catal. Lett.* **1998**, *54*, 171−176.
(22) Boucher, M. B.; Zugic, B.; Cladaras, G.; Kammert, J.; Marcinkowski, M. D.; Lawton, T. J.; Sykes, E. C. H.; Flytzani-Stephanopoulos, M. Single Atom Alloy Surface Analogs in Pd0.18 Cu15 Nanoparticles for Selective Hydrogenation Reactions. *Phys. Chem. Chem. Phys.* **2013**, *15* (29), 12187−12196.
(23) Liu, J.; Lucci, F. R.; Yang, M.; Lee, S.; Marcinkowski, M. D.; Therrien, A. J.; Williams, C. T.; Sykes, E. C. H.; Flytzani-Stephanopoulos, M. Tackling CO Poisoning with Single-Atom Alloy Catalysts. *J. Am. Chem. Soc.* **2016**, *138* (20), 6396−6399.
(24) Huber, G. W.; Iborra, S.; Corma, A. Synthesis of Transportation Fuels from Biomass: Chemistry, Catalysts, and Engineering. *Chem. Rev.* **2006**, *106*, 4044−4098.
(25) Cai, C. M.; Nagane, N.; Kumar, R.; Wyman, C. E. Coupling Metal halides with a Co-solvent to Produce Furfural and 5-HMF at High Yields Directly from Lignocellulosic Biomass as an Integrated Biofuels Strategy. *Green Chem.* **2014**, *16*, 3819−3829.
(26) Bohre, A.; Dutta, S.; Saha, B.; Abu-Omar, M. M. Upgrading Furfurals to Drop-in Biofuels: An Overview. *ACS Sustainable Chem. Eng.* **2015**, *3* (7), 1263−1277.
(27) Li, G.; Li, N.; Li, S.; Wang, A.; Cong, Y.; Wang, X.; Zhang, T. Synthesis of Renewable Diesel with Hydroxyacetone and 2-Methyl furan. *Chem. Commun.* **2013**, *49* (51), 5727−5729.
(28) Li, G.; Li, N.; Wang, X.; Sheng, X.; Li, S.; Wang, A.; Cong, Y.; Wang, X.; Zhang, T. Synthesis of Diesel or Jet Fuel range Cycloalkanes with 2-Methylfuran and Cyclopentanone from Lignocellulose. *Energy Fuels* **2014**, *28* (8), 5112−5118.
(29) Wang, J.; Liu, X.; Hu, B.; Lu, G.; Wang, Y. Efficient Catalytic Conversion of Lignocellulosic Biomass into Renewable Liquid Biofuels via Furan Derivatives. *RSC Adv.* **2014**, *4* (59), 31101−31107.
(30) Srivastava, S.; Jadeja, G. C.; Parikh, J.; Alonso, D. M.; Wettstein, S. G.; Dumesic, J. A.; Datta, S.; De, S.; Saha, B.; Alam, I.; et al. A Versatile Bi-metallic Copper−Cobalt Catalyst for Liquid Phase hydrogenation of Furfural to 2-Methylfuran. *RSC Adv.* **2016**, *6* (2), 1649−1658.
(31) Aldosari, O. F.; Iqbal, S.; Miedziak, P. J.; Brett, G. L.; Jones, D. R.; Liu, X.; Edwards, J. K.; Morgan, D. J.; Knight, D. K.; Hutchings, G. J. Pd-Ru/TiO2 Catalyst - an Active and Selective Catalyst for Furfural Hydrogenation. *Catal. Sci. Technol.* **2016**, *6* (1), 234−242.
(32) Garcia-Olmo, A. J.; Yepez, A.; Balu, A. M.; Romero, A. A.; Li, Y.; Luque, R. Insights into the Activity, Selectivity and Stability of Heterogeneous Catalysts in the Continuous Flow Hydroconversion of Furfural. *Catal. Sci. Technol.* **2016**, *6* (13), 4705−4711.
(33) Scholz, D.; Aellig, C.; Hermans, I. Catalytic Transfer Hydrogenation/Hydrogenolysis for Reductive Upgrading of Furfural and 5-(Hydroxymethyl)furfural. *ChemSusChem* **2014**, *7* (1), 268−275.
(34) Luo, J.; Monai, M.; Yun, H.; Arroyo-Ramírez, L.; Wang, C.; Murray, C. B.; Fornasiero, P.; Gorte, R. J. The H2 Pressure Dependence of Hydrodeoxygenation Selectivities for Furfural over Pt/C Catalysts. *Catal. Lett.* **2016**, *146* (4), 711−717.
(35) Vargas-Hernández, D.; Rubio-Caballero, J. M.; Santamaría-González, J.; Moreno-Tost, R.; Mérida-Robles, J. M.; Pérez-Cruz, M. A.; Jiménez-López, A.; Hernández-Huesca, R.; Maireles-Torres, P. Furfuryl alcohol from Furfural Hydrogenation over Copper Supported on SBA-15 Silica Catalysts. *J. Mol. Catal. A: Chem.* **2014**, *383−384*, 106−113.
(36) Yan, K.; Chen, A. Selective Hydrogenation of Furfural and Levulinic acid to Biofuels on the Ecofriendly Cu-Fe Catalyst. *Fuel* **2014**, *115*, 101−108.
(37) Sheng, H.; Lobo, R. F. Iron-Promotion of Silica-Supported Copper Catalysts for Furfural Hydrodeoxygenation. *ChemCatChem* **2016**, *8* (21), 3402−3408.
(38) Kyriakou, G.; Boucher, M. B.; Jewell, A. D.; Lewis, E. a.; Lawton, T. J.; Baber, A. E.; Tierney, H. L.; Flytzani-stephanopoulos, M.; Sykes, E. C. H. Isolated Metal Atom Geometries as a Strategy for Selective

DOI: 10.1021/acssuschemeng.7b03572
ACS Sustainable Chem. Eng. XXXX, XXX, XXX−XXX

Heterogeneous Hydrogenations. *Science (Washington, DC, U. S.)* **2012**, *335* (6073), 1209−1212.
(39) Seemala, B.; Cai, C. M.; Wyman, C. E.; Christopher, P. Support Induced Control of Surface Composition in Cu-Ni/TiO2 Catalysts Enables High Yield Co-Conversion of HMF and Furfural to Methylated Furans. *ACS Catal.* **2017**, *7* (6), 4070−4082.
(40) Larsson, P. O.; Andersson, A. Complete Oxidation of CO, Ethanol, and Ethyl Acetate over Copper Oxide Supported on Titania and Ceria Modified Titania. *J. Catal.* **1998**, *179* (1), 72−89.
(41) Han, K.; Kreuger, T.; Mei, B.; Mul, G. Transient Behavior of Ni@NiOx Functionalized SrTiO3 in Overall Water Splitting. *ACS Catal.* **2017**, *7* (3), 1610−1614.
(42) Sitthisa, S.; Sooknoi, T.; Ma, Y.; Balbuena, P. B.; Resasco, D. E. Kinetics and Mechanism of Hydrogenation of Furfural on Cu/SiO2 Catalysts. *J. Catal.* **2011**, *277*, 1−13.
(43) Li, X.; Jia, P.; Wang, T. Furfural: A Promising Platform Compound for Sustainable Production of C4 and C5 Chemicals. *ACS Catal.* **2016**, *6*, 7621−7640.
(44) Dunlop, A. P.; Fredus N, P. Thermal Stability of Furfural. *Ind. Eng. Chem.* **1940**, *32* (12), 1639−1641.
(45) Ghasemi, B.; Anvaripour, B.; Jorfi, S.; Jaafarzadeh, N. Enhanced Photocatalytic Degradation and Mineralization of Furfural Using UVC/TiO2/GAC Composite in Aqueous Solution. *Int. J. Photoenergy* **2016**, *2016*, 1−10.
(46) Naghash, A. R.; Etsell, T. H.; Xu, S. XRD and XPS Study of Cu - Ni Interactions on Reduced Copper - Nickel - Aluminum Oxide Solid Solution Catalysts. *Chem. Mater.* **2006**, *18* (10), 2480−2488.
(47) Kloet, S. C.; Sachtler, W. M. H. Study of Copper-Nickel Alloy Formation on Silica Supports by the Magnetostatic and Other Methods. *J. Catal.* **1975**, *39*, 234−248.
(48) Wu, J.; Gao, G.; Li, J.; Sun, P.; Long, X.; Li, F. Efficient and Versatile CuNi Alloy Nanocatalysts for the Highly Selective Hydrogenation of Furfural. *Appl. Catal., B* **2017**, *203*, 227−236.
(49) Lin, J.; Biswas, P.; Guliants, V. V.; Misture, S. Applied Catalysis A : General Hydrogen production by Water − Gas Shift Reaction over Bimetallic Cu-Ni Catalysts Supported on La-doped mesoporous ceria. *Appl. Catal., A* **2010**, *387*, 87−94.
(50) Zhang, L.; Liu, J.; Li, W. Ethanol Steam Reforming over Ni-Cu/Al2O3-MyOz (M = Si, La, Mg, and Zn) Catalysts. *J. Nat. Gas Chem.* **2009**, *18*, 55−65.

DOI: 10.1021/acssuschemeng.7b03572
ACS Sustainable Chem. Eng. XXXX, XXX, XXX−XXX